Numerical Simulation of the Effect of Shock Strength on Normal Shock/Homogeneous Turbulence Interaction

Mohammad Ali Jinnah* and Kazuyoshi Takayama**

ABSTRACT

Shock wave interactions with grid-generated homogeneous and isotropic turbulence are observed numerically by solving the time-dependent three-dimensional Navier-Stokes equations with k-ε turbulence model for a compressible fluid. Numerical measurements are taken before and after the interaction of turbulent regime with the normal shock wave reflected from the end wall. All turbulent fluctuations are measured during the compression by the reflected shock on the turbulent field and it is observed that the longitudinal turbulent velocity fluctuations are amplified after the shock/turbulence interaction. The amplification of turbulent fluctuations and turbulent kinetic energy level depend on the shock strength and the shock induced flow conditions behind the shock wave. The amplification factor of longitudinal turbulence intensity is 1.985-2.120 and the amplification factor of turbulent kinetic energy level is 3.086-3.410 in interaction of normal shock with homogeneous, isotropic turbulence for incident shock Mach number 1.50 and the amplification magnitude of longitudinal turbulence intensity and turbulent kinetic energy level decrease for incident shock Mach number 2.20 where the dissipation rate of turbulent kinetic energy decrease in all the cases of shock/turbulence interaction.

Keywords: *Shock wave, Turbulent flow, Navier-Stokes equations, Turbulence model, Shock /turbulence interaction*

* *MCE Department, Islamic University of Technology, Board Bazar, Gazipur-1704*
** *Multidisciplinary Shock Wave Research Center, Tohoku University, 2-1-1 katahira, Aoba-ku, Sendai 980-8577, Japan*
E-mail: jinnah@iut-dhaka.edu

1 INTRODUCTION

The interaction of shock waves with turbulent flows is of great practical importance in engineering applications. These types of interactions are commonly seen in aeromechanical systems and in combustion processes as well as in high-speed rotor flows. For designing aero-mechanism systems such as transport aircraft of supersonic and hypersonic speed, the shock wave and the turbulence interaction effects are the important phenomena. The outcomes of the interactions of shock wave with homogeneous and isotropic turbulence are the amplification of longitudinal velocity fluctuation, the amplification of turbulent kinetic energy level and substantial changes in length scales. The selection of homogeneous and isotropic turbulent field interactions are the easier phenomena than the other types of turbulent field like turbulent boundary layer interactions, turbulent wake-shock interaction etc. Turbulence amplification through shock wave interactions is a direct effect of the Rankine-Hugoniot relations.

For the present numerical investigations, it is attempted to generate a compressible flow of homogeneous, isotropic turbulence in a shock tube. The shock wave and the gas flow following the shock are passed through the turbulence grid. The elementary waves formed by diffraction of the shock at the grid propagate in downstream direction and after a short period converge to form again plane, normal shock which is weaker than the incident shock. The plane shock after the reflection from the end wall of the tube interacts with the grid-generated turbulent field. In these computations, the shock induced flow velocities behind the incident shock are subsonic flow and supersonic flow. After passing the turbulence-generating grids, the flow oscillations increase and the flow velocity inside the selected turbulent field are less than the initial flow velocity. The flow velocities behind the reflected shock are very low and the turbulent field oscillations increase after the interaction with the reflected shock. The aim of the numerical measurements is to compare the turbulent properties of this flow regime before and after the interaction with the reflected shock wave. The reflected shock is plane in shape at the beginning of the interaction and due to interaction with the turbulent field, the shock wave starts distorted whose magnitude depends on the strength of the turbulent field. The flow velocities are changed from subsonic flow to supersonic flow by increasing the shock Mach number to observe the basic change of the turbulent field after the interaction. In these computations, three-dimensional numerical code are selected because all of the interactions are three dimensional in nature and turbulence in all its complexity is characterized by instantaneous flow variables that exhibits a variations in time and space.

Experimental realization of a homogeneous and isotropic flow interacting with a normal shock in the laboratory is a difficult task due to generation of compressible and isotropic turbulent flow and the generation of a normal shock interacting with flow. The experimental arrangement in shock tubes offers the possibility of unsteady shock interactions with isotropic turbulence of various length scale and intensity. Such types of experiments were conducted by Hesselink and Sturtevant [1], Keller and Merzkirch [2], Honkan and Androupoulus [3]. Configuring a homogeneous and isotropic turbulence interacting with a normal shock in a supersonic wind tunnel appears to be more difficult than in a shock tube. A turbulence-generating grid or other device is usually placed in the flow upstream of the converging-diverging nozzle. The flow then interacts with a stationary shock produced by a suitable section. The problem with such configurations is that the flow anisotropy is substantially increased through the nozzle. A multi nozzle turbulence generator was used in the Mach 3 experiments of Alem [4] published by Barre et al. [5]. A normal shock was formed by the interaction of two oblique shock waves of opposite directions. The flow after the interaction is highly accelerated because of the two-shear layers/slip lines in the boundary of the useful flow region. The velocity is 200m/s at x=10 mm after the shock and increases to 250m/s at 20mm, which results in an acceleration of $\delta u/\delta x$=5400s^{-1}. This level of acceleration is very strong and is expected to reduce turbulence intensities after the interaction. Thus, the amplification levels found in this work are probably contaminated by the additional effects of acceleration in the subsonic flow downstream of the interaction. Another weakness of this data set is that the level of turbulence intensity at the location of the shock is extremely low, ~0.4%.

Experiments on the interaction between the shock wave and the grid-generated turbulence were conducted by Debreve and Lacharme [6] and they measured velocity and temperature spectra upstream and downstream of the shock wave and concluded that turbulent fluctuations are amplified and Taylor micro scales increase during the interaction. Jacquin et al. [7] investigated the interactions of a normal shock wave with grid-generated turbulence and a turbulent jet and they observed that turbulence amplification was not significant for the grid-generated turbulence and that the decay of turbulent kinetic energy was accelerated downstream of the shock wave. Their experiments treated the interaction of a shock with quasi-incompressible turbulence where fluctuations in pressure and density are not significant. An experiment on the interaction of weak shocks (M_s=1.007, 1.03 and 1.1) with a random medium of density in homogeneity was performed by Hesselink and Sturtevant [1]. They observed that the pressure histories of the distorted shock waves were both peaked and rounded and explained these features in terms of the focusing/defocusing of the shock front due to in homogeneity of the medium.

Numerical technique for such types of interactions is more suitable to get the reliable results and easily estimate the physical data structure which can difficult to measure in experiment. Using a shock capturing numerical technique, Rotman [8] numerically calculated the change in a two-dimensional turbulent flow caused by the passage of a traveling shock wave. He found that the shock causes in increase in the turbulent kinetic energy and that the length scale of the turbulent field is reduced upon passage of the shock. He also found that increasing the initial turbulent kinetic energy caused a straight shock wave to evolve into a distorted front. Lee, Lele and Moin [9] conducted direct numerical simulations of two-dimensional turbulence interacting with a shock wave and found that vorticity amplification compared well with the predictions of the linear analysis but turbulent kinetic energy evolution behind the shock showed significant nonlinear effects. The energy spectrum was found to be enhanced more at large wave numbers, leading to an overall length scale decrease. For the present numerical simulation, the 3D Navier-stokes equations using k-ε turbulence model, are solved by shock capturing method where for more accurate solutions, the grid adaptation techniques are used. Grid adaptation techniques with k-ε turbulence model are the improve techniques for numerical simulation of shock/turbulence interaction.

2 NUMERICAL METHODS

The three-dimensional unsteady, compressible, Reynolds-averaged Navier-Stokes equations with k-ε turbulence model are solved by shock capturing method. Without external forces and heat sources, the conservative form of non-dimensionalized governing equation in three-dimensional Cartesian coordinate system is,

$$\frac{\partial Q}{\partial t}+\frac{\partial (F-Fv)}{\partial x}+\frac{\partial (G-Gv)}{\partial y}+\frac{\partial (H-Hv)}{\partial z}=S(Q)$$

where, $Q=[\rho,\ u,\ v,\ w,\ e,\ k,\ \varepsilon\ ]$, t is the time, F, G & H are inviscid flux vectors and F_v, G_v & H_v are viscous flux vectors and $S(Q)$ is the source term of k-ε model. Also ρ is the fluid density and u, v and w are velocity components in each direction of Cartesian coordinates. e is the total energy per unit volume.

The governing equations described above for compressible viscous flow are discretised by the finite volume method. An upwind Godounov scheme of Flux vector splitting method is used to discrete the inviscid flux terms and MUSCL-Hancock scheme with k-ε turbulence model is used for interpolation of variables where HLL Reimann solver is used for shock capturing in the flow. Central differencing scheme is used in discretizing the viscous flux terms. Two equations for k-ε turbulence model are used to determine the dissipation of turbulent kinetic energy and the rate of dissipation. The k and ε equations, each contains nonlinear production and destruction source terms, which can be very large near the solid boundaries. According to linear stability theory, such terms can also severely reduce convergence rates if purely explicit scheme is used to descretize the equations.

Three dimensional hexahedral cells with adaptive grids are used for these computations. In the grid system, the cell-edge data structures are arranged in such a way that each cell contains six faces which are sequence in one to six and each face indicates two neighboring cell that is left cell and right cell providing all faces of a cell are vectorized by positions and coordinates. The initial three-dimensional mesh with turbulence-generating grids is shown in Fig.1. The physical size of each cell before adaptation is 5 x 5 x 5 *(mm)* and the initial number of cell is 1985. For the computations, the grid adaptation is performed by two procedures, one is refinement procedure and another is coarsening procedure. In the refinement procedure, the cells are selected for refinement in which every cell is divided into eight new sub cells and these new sub cells are arranged in a particular sequence so that these sub cells are used suitably in the data-structure. In three-dimensional adaptation, the volume of new sub cells is 1/8 of primary cell where in two-dimensional, this fraction is 1/4. In the coarsening procedure, the eight

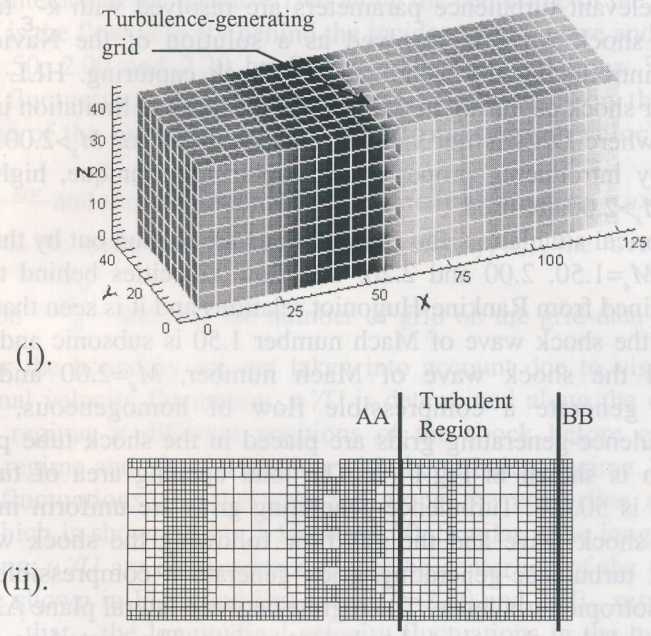

Figure 1: (i) Three dimensional grid systems and turbulence-generating grids. (ii) Sectional view of adaptive *ZX*-plane where the turbulent regime is shown.

sub cells, which are generated from the primary cell, are restored into primary cell. The refinement and coarsening operations are handled separately in the computation. The refinement and coarsening operations depend on the threshold values for refinement and coarsening. In these computations, the threshold values for refinement are used 0.16~0.48 and the threshold values for coarsening are

used 0.12~0.44 and the higher values are used for higher shock Mach number and the level of refinement is 2. The adaptive mesh systems are shown in Fig.1 (ii), which are the two-dimensional cross sectional view of *ZX*-plane. The above three-dimensional adaptive strategy is an extension and upgraded works of the two-dimensional code (e.g. Sun [10]).

The upstream of incident shock wave is set as an inflow boundary condition, the properties and velocities of which are calculated from Rankine-Hugoniot conditions with incident shock Mach number. The downstream inflow boundary condition and the wall surface are used as solid boundary conditions where the gradients normal to the surface are taken zero. All solid walls are treated as viscous solid wall boundary. For the two-equation k-ε model on solid boundaries, turbulent eddy viscosity, μ_t is set to zero.

3 RESULTS AND DISCUSSION

In these computations, the time-dependent Navier-Stokes equations with k-ε turbulence model for a compressible fluid are solved by grid adaptation technique. All relevant turbulence parameters are resolved with k-ε turbulence model and the shock wave is resolved as a solution of the Navier-Stokes equations with introducing the techniques of shock capturing. HLL Reimann solver is used for shock capturing in the flow. There has one limitation in DNS of Lee et al. [11] where DNS is not valid in a shock wave for M_s>2.00. In these computations, by introducing proper shock capturing technique, higher shock Mach number, M_s>2.00 are used.

For the numerical simulation, the computations are carried out by three shock Mach number, M_s=1.50, 2.00 and 2.20. The flow velocities behind the shock wave are determined from Rankine-Hugoniot relations and it is seen that the flow velocity behind the shock wave of Mach number 1.50 is subsonic and the flow velocity behind the shock wave of Mach number, M_s=2.00 and 2.20 is supersonic. To generate a compressible flow of homogeneous, isotropic turbulence; turbulence-generating grids are placed in the shock tube parallel to *YZ* plane, which is shown in Fig.1 (i). The total opening area of turbulence-generating grids is 50.6%. Turbulence-generating grids are uniform in size and spacing; so the shock wave and the gas flow following the shock wave after passing through turbulence-generating grids generate a compressible flow of homogeneous, isotropic turbulence. The regime between lateral plane AA and BB in Fig.1 (ii), is treated as the selected turbulent regime. The centerline, along the longitudinal direction of turbulent regime is treated as the centerline of the turbulent regime. 20 points of equal spacing are taken on the centerline of the turbulent regime and all turbulent parameters (velocity fluctuations, pressure fluctuations etc.) are computed on these 20 points. The lateral planes intersect these points and parallel to the *YZ* plane are treated as grid-data plane and the grids inside the turbulent regime cut by the grid-data plane are the grids on the grid-data plane. The value of the turbulent parameter on the center line of the

turbulent regime is the average value of all the grid value of that parameter on the grid-data plane and in these computations, the grids adjacent to the boundary are not taken into account due to viscous effect. All the relevant turbulent parameters are determined along the centerline of the turbulent regime at the moment of reflected shock before entering into the turbulent regime and after interaction with the turbulent regime. The fluctuations before interaction are measured for different positions of shock between the turbulent regime and the end wall. The different positions of shock before interaction between the turbulent regime and the end wall are, first position is before reflection from the end wall and near the end wall that is far from the turbulent regime, second position is after reflection from the end wall and near the end wall that is far from the turbulent regime and third position is after reflection from the end wall and near the turbulent regime. The longitudinal distances (X/m) of any point on the centerline of the turbulent regime are determined from the turbulence-generating gird where m is the maximum dimensional length of a grid in the grid systems.

The dimensionless longitudinal velocity fluctuations (u'/U) before interaction and after interaction are characterized along the centerline of the turbulent regime where, U is the flow velocity behind the incident shock wave and it is determined for M_s=1.50, 2.00 and 2.20 by Rankine–Hugoniot relations. The longitudinal velocity fluctuations (u') are the average fluctuation on the points of the centerline of the turbulent regime. The longitudinal velocity fluctuation, $u' = \frac{\sum_{i=1}^{n} |u_i - u_{av}|}{n}$ and the longitudinal RMS velocity fluctuation, $\langle u \rangle = \sqrt{\frac{\sum_{i=1}^{n} (u_i - u_{av})^2}{n}}$ where, u_i is the instantaneous longitudinal velocity, u_{av}, the average velocity in X-direction $= \frac{\sum_{i=1}^{n} u_i}{n}$ and n is the number of grid on the grid-data plane where the grids near the boundary are not taken into account due to viscous effect. The longitudinal velocity fluctuation, u'/U is determined along the centerline of the turbulent regime at different positions of the shock before entering into the turbulent regime and after interaction with the turbulent regime. The longitudinal velocity fluctuations are characterized along the centerline of the turbulent regime which is shown in Fig.2 for M_s=1.50. Similarly the longitudinal velocity fluctuations, u'/U are characterized along the centerline of the turbulent regime which are shown in Fig.3 and Fig.4, for M_s=2.00 and 2.20 respectively. It is observed that the longitudinal velocity fluctuations in the turbulent field are enhanced during the compression by the reflected shock on the turbulent field. The RMS longitudinal turbulence intensity, $\langle u \rangle/U$ before interaction and after interaction are determined along the centerline of the turbulent regime for M_s= 1.50, 2.00 and 2.20. The outcomes of interaction are the amplification of RMS longitudinal turbulence intensity and the amplification factor is defined by $\frac{\langle u \rangle_{after\_interaction}}{\langle u \rangle_{before\_interaction}}$. The variation of amplification factor of longitudinal turbulence intensity for different shock Mach number is shown in Fig.5. It

is shown that the amplification range of longitudinal turbulence intensity is from 1.162 to 2.399 for Mach number range from 1.50 to 2.20. The experimental data of Honkan et al. [12] for shock Mach number, M_s= 1.354 shows that the amplification factor varies from 1.1 to 1.48. In these computations, the amplification factor of turbulence intensity for M_s=1.50 varies from 1.985 to 2.120 where the fluctuations are measured after reflection from the end wall. Similarly for M_s=2.00, it varies from 1.352 to 1.441 and for M_s=2.20, it varies from 1.162 to 1.223 where the fluctuations are measured after reflection from the end wall. The highest amplification of turbulence intensity is 2, which is observed in the experimental data of Briassulis and Andreopoulos [13]. From the results of LIA data of Lee et al. [11], the maximum amplification of turbulence intensity is close to 2.00 for Mach number range 1.02 to 1.2. From these computations, it is clear that the outcomes of interaction effect of shock wave with the subsonic flow are more than the outcomes of interaction effect of shock wave with the supersonic flow and it is observed that inside the turbulent regime, the fluctuations after reflection are enhanced more than the fluctuations at the moment of reflection.

The lateral velocity fluctuation, $v' = \frac{\sum_{i=1}^{n} |v_i - v_{av}|}{n}$ where, v_i is the instantaneous lateral velocity in Y-direction, v_{av} , is the average velocity in Y-direction $= \frac{\sum_{i=1}^{n} v_i}{n}$ and n is the number of grid on the grid-data plane where the grids near the boundary are not taken into account due to viscous effect. Similarly, the lateral velocity fluctuation, $w' = \frac{\sum_{i=1}^{n} |w_i - w_{av}|}{n}$ and where, w_i is the instantaneous lateral velocity in Z-direction, the average velocity, $w_{av} = \frac{\sum_{i=1}^{n} w_i}{n}$, in Z-direction and n is the number of grid on the grid-data plane where the grids near the boundary are not taken into account due to viscous effect. It is observed that no substantial amplification of the lateral velocity fluctuation occurs after interaction. The characteristics behaviors of v' are almost identical with the characteristics behaviors of w', which was explained by Barre et al. [5] and confirmed that the v' and w' components behave in the same way across the shock.

The normalized pressure variation along the centerline of the turbulent regime are determined by P_{av}/P_o where the average pressure, $P_{av} = \frac{\sum_{i=1}^{n} p_i}{n}$, p_i is the instantaneous pressure for any grid on the grid-data plane and n is the number of grid on the grid-data plane avoiding grids near the boundary. P_o is the STD atmospheric pressure. It is observed that no substantial pressure variations occur along the centerline of the turbulent regime. The pressure fluctuation,

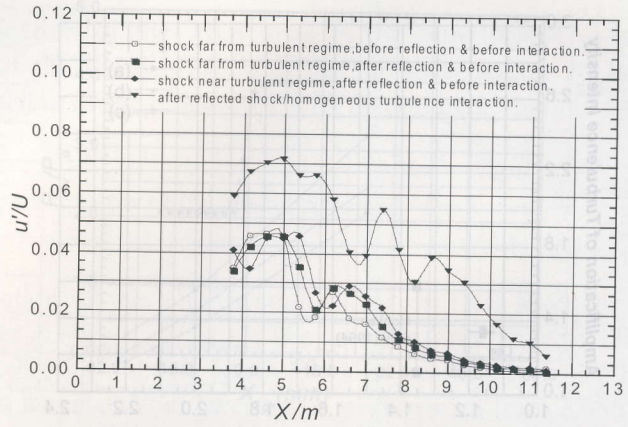

Figure 2: Longitudinal velocity fluctuation *(u'/U)* profile along the centerline of turbulent regime where M_s=1.50.

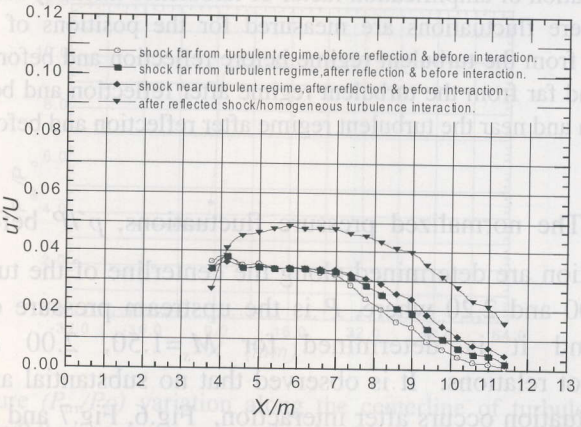

Figure 3: Longitudinal velocity fluctuation *(u'/U)* profile along the centerline of turbulent regime where M_s=2.00.

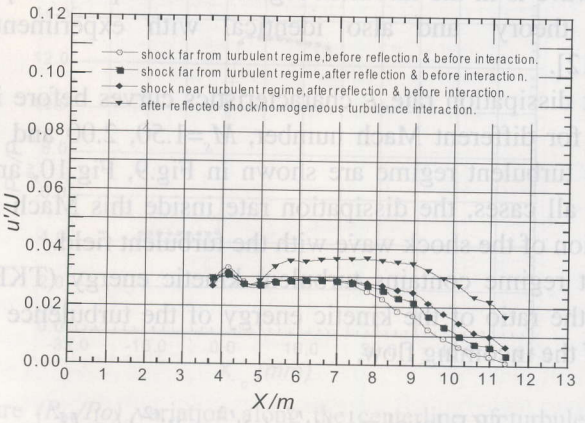

Figure 4: Longitudinal velocity fluctuation *(u'/U)* profile along the centerline of turbulent regime where M_s=2.20.

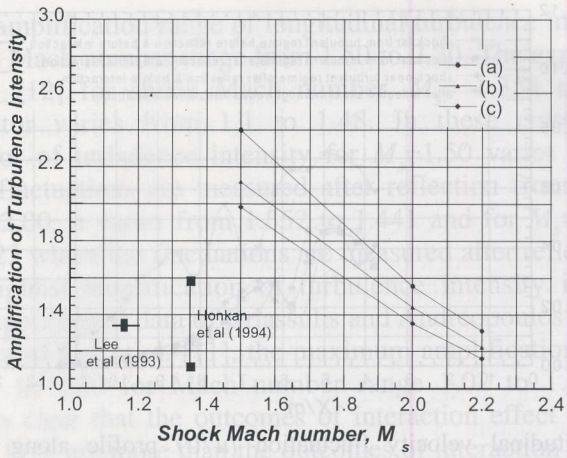

Figure 5: The variation of amplification factor of turbulence intensity for different shock Mach number where fluctuations are measured for the positions of shock (a) after interaction and far from the turbulent regime before reflection and before interaction (b) after interaction and far from the turbulent regime after reflection and before interaction (c) after interaction and near the turbulent regime after reflection and before interaction.

$p' = \frac{\sum_{i=1}^{n} |p_i - p_{av}|}{n}$. The normalized pressure fluctuations, p'/P before interaction and after interaction are determined along the centerline of the turbulent regime for M_s=1.50, 2.00 and 2.20 where, P is the upstream pressure of the incident shock wave and it is determined for M_s=1.50, 2.00 and 2.20 by Rankine–Hugoniot relations. It is observed that no substantial amplification of the pressure fluctuation occurs after interaction. Fig.6, Fig.7 and Fig.8 show the pressure variations across the reflected shock wave when the position of the reflected shock wave is in the turbulent regime and the pressure profile obey the shock reflection theory and also identical with experimental results of Honkan et al. [12].

The turbulent dissipation rate, ε characteristics curves before interaction and after interaction for different Mach number, M_s=1.50, 2.00 and 2.20 along the centerline of the turbulent regime are shown in Fig.9, Fig.10, and Fig.11. It is observed that in all cases, the dissipation rate inside this Mach range decrease after the interaction of the shock wave with the turbulent field.

The turbulent regime contains turbulent kinetic energy (TKE) levels. TKE level represents the ratio of the kinetic energy of the turbulence divided by the kinetic energy of the incoming flow,

$$\text{TKE level} = \tfrac{1}{2}\,(u'^2 + v'^2 + w'^2) / \tfrac{1}{2}\,U^2$$

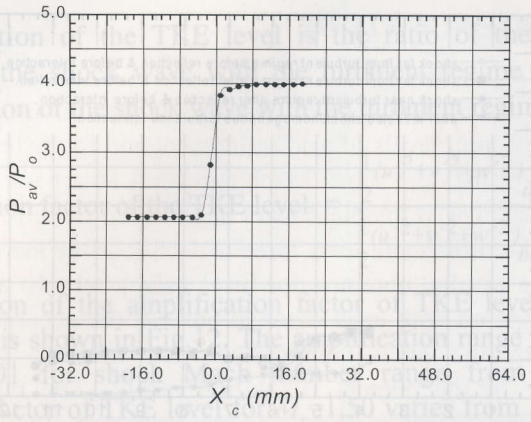

Figure 6: Pressure (P_{av}/Po) variation along the centerline of turbulent regime where M_s=1.50 (Here X_c=0.0 mm corresponds to the shock location and X/m=7.6).

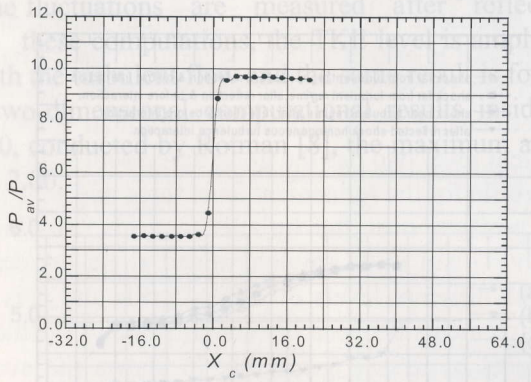

Figure 7: Pressure (P_{av}/Po) variation along the centerline of turbulent regime where M_s=2.00 (Here X_c=0.0 mm corresponds to the shock location and X/m=7.2).

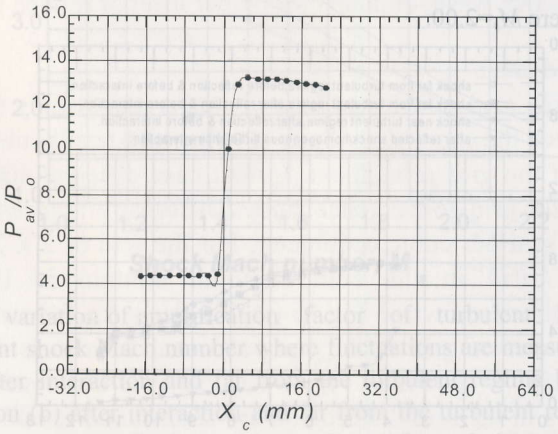

Figure 8: Pressure (P_{av}/Po) variation along the centerline of turbulent regime where M_s=2.20 (Here X_c=0.0 mm corresponds to the shock location and X/m=7.2).

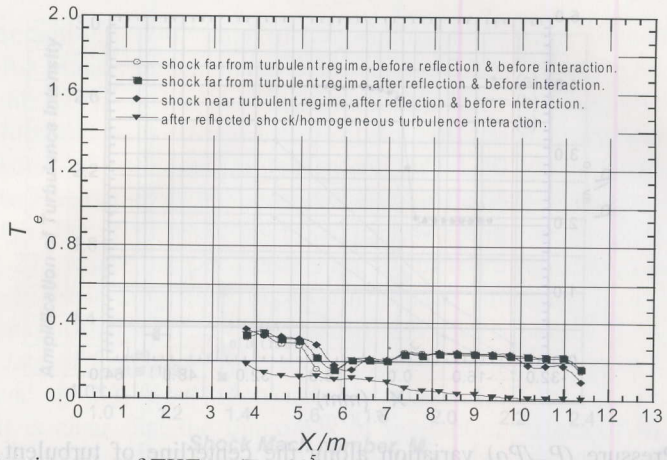

Figure 9: Dissipation rate of TKE, ε $(T_e=10^5\varepsilon)$ variations along the centerline of the turbulent regime where M_s=1.50.

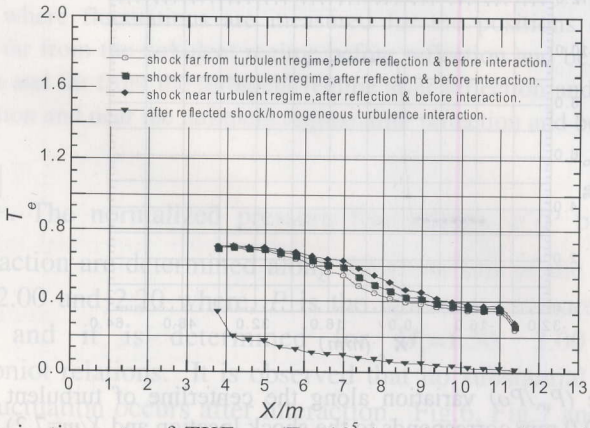

Figure 10: Dissipation rate of TKE, ε $(T_e=10^5\varepsilon)$ variations along the centerline of the turbulent regime where M_s=2.00.

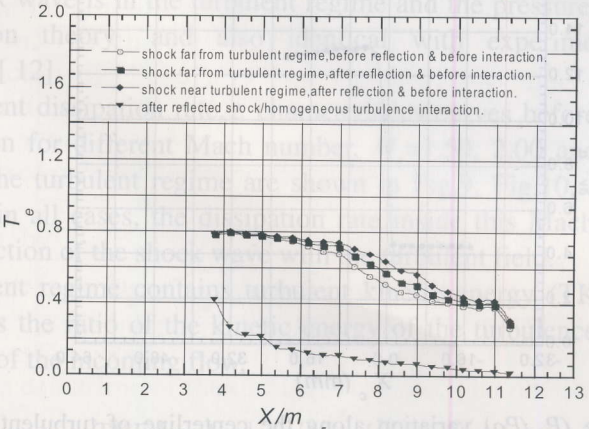

Figure 11: Dissipation rate of TKE, ε $(T_e=10^5\varepsilon)$ variations along the centerline of the turbulent regime where M_s=2.20.

The amplification of the TKE level is the ratio of the average TKE after interaction of the shock wave with the turbulent regime to the average TKE before interaction of the shock wave with the turbulent regime.

$$\text{The amplification factor of the TKE level} = \frac{\frac{1}{2}(u'^2+v'^2+w'^2)_{after\ interaction}}{\frac{1}{2}(u'^2+v'^2+w'^2)_{before\ interaction}}$$

The variation of the amplification factor of TKE level for different shock Mach number is shown in Fig.12. The amplification range of TKE level is from 1.655 to 3.901 for shock Mach number range from 1.50 to 2.20. The amplification factor of TKE level for M_s=1.50 varies from 3.086 to 3.410 where the fluctuations are measured after reflection from the end wall. Similarly for M_s=2.00, it varies from 1.999 to 2.136 and for M_s=2.20, it varies from 1.655 to 1.752 where the fluctuations are measured after reflection from the end wall. So in these computations, the TKE level is amplified in interaction of shock wave with the turbulent flow and the same result is found in DNS of Lee et al [11]. The two-dimensional computational results inside the Mach number range 1.01-1.50, conducted by Rotman [8], the maximum amplification factor of TKE level was 2.00.

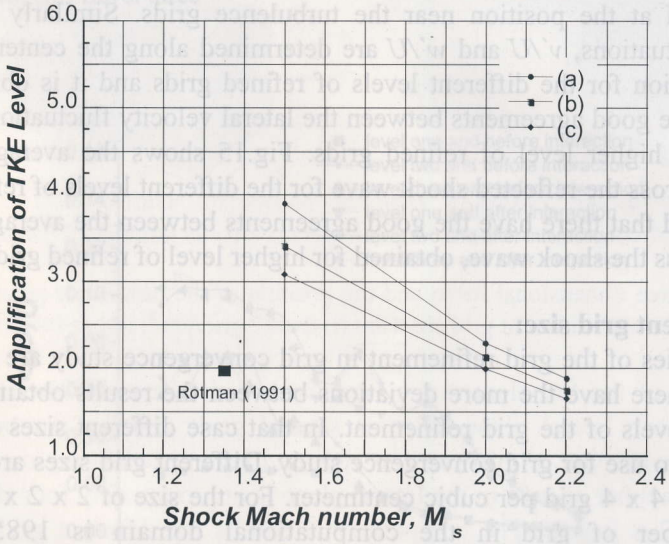

Figure 12: The variation of amplification factor of turbulent kinetic energy (TKE) level for different shock Mach number where fluctuations are measured for the positions of shock (a) after interaction and far from the turbulent regime before reflection and before interaction (b) after interaction and far from the turbulent regime after reflection and before interaction (c) after interaction and near the turbulent regime after reflection and before interaction.

4 GRID CONVERGENCE STUDY

Using different level of refined grid:

The study of the grid convergence on the present computational results has been carried out for different levels of grid refinement and for different grid sizes. The results, obtained for incident shock Mach number 1.50 are used for the study of the grid convergence. The refinement level one is used to solve the flow field with coarse grid and the refinement level three is used to solve the flow field with very refined grid. The results, obtained for level one, level two and level three refined grids, are compared with each other to observe the accuracy level of the computational results and such comparisons are used to determine the convergence behavior of the present simulation results. The two-dimensional sectional views of adaptive grids of refinement level one, two and three are shown in Fig.13. The RMS (Root Mean Square) value of longitudinal velocity fluctuations or the longitudinal turbulence intensity, $<u>/U$ are determined along the centerline of the turbulent region for the different levels of refined grids which is shown in Fig.14. It is observed that the longitudinal turbulence intensity profile, obtained from the refinement level one, has some deviations with the profiles for higher refinement level and the longitudinal turbulence intensity profile for the refinement level two has the good agreement with the longitudinal turbulence intensity profile for the refinement level three and some disagreements are observed at the position near the turbulence grids. Similarly the lateral velocity fluctuations, v'/U and w'/U are determined along the centerline of the turbulent region for the different levels of refined grids and it is observed that there have the good agreements between the lateral velocity fluctuations profiles, obtained for higher level of refined grids. Fig.15 shows the average pressure variations across the reflected shock wave for the different levels of refined grids. It is observed that there have the good agreements between the average pressure profiles across the shock wave, obtained for higher level of refined grids.

Using different grid size:

The utilities of the grid refinement in grid convergence study are sometimes difficult if there have the more deviations between the results obtained by two successive levels of the grid refinement. In that case different sizes of the grid are suitable to use for grid convergence study. Different grid sizes are 2 x 2 x 2 grid and 4 x 4 x 4 grid per cubic centimeter. For the size of 2 x 2 x 2 grid, the initial number of grid in the computational domain is 1985 and the computational domain is shown in Fig.16 (i). Similarly for the size of 4 x 4 x 4 grid, the initial number of grid in the computational domain is 15880 and the computational domain is shown in Fig.16 (ii). So it is observed that different turbulent parameters in the turbulent region are determined for different number and size of the grids contain in the turbulent region. The lateral planes intersect

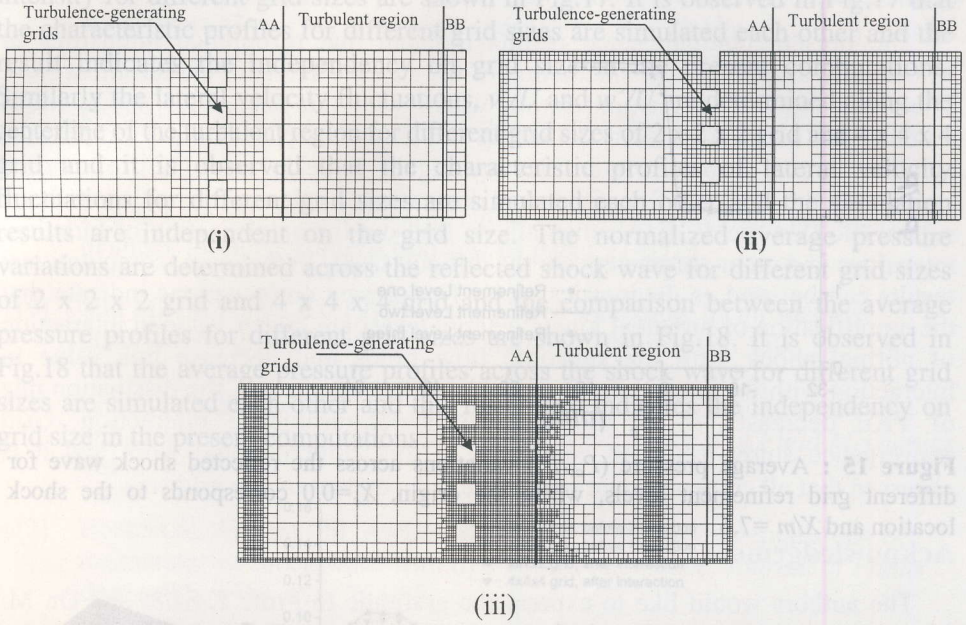

Figure 13: Two-dimensional cuts of the three-dimensional adaptive grids: (i) Level one; (ii) Level two; (iii) Level three

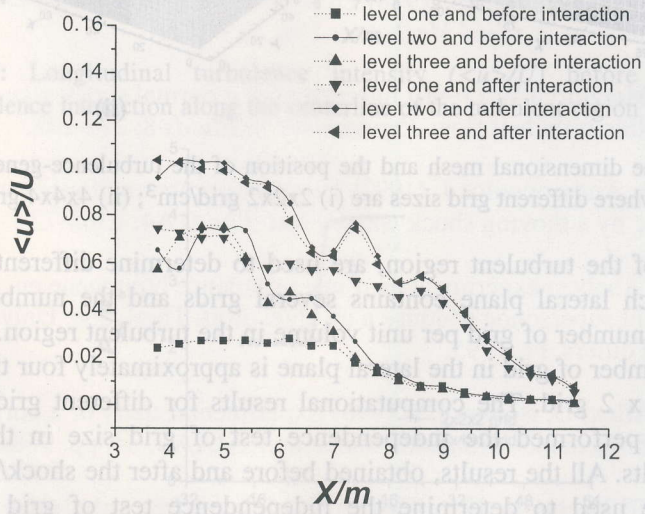

Fig.14 Longitudinal turbulence intensity ($<u>/U$) before and after the shock/turbulence interaction along the centerline of the turbulent region for different grid refinement levels

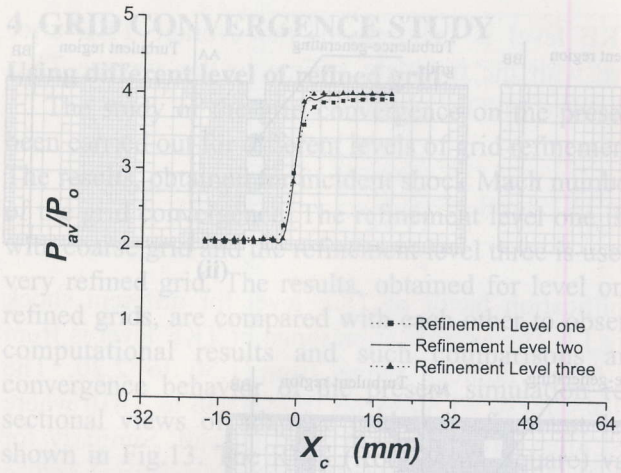

Figure 15 : Average pressure (P_{av}/P_o) variations across the reflected shock wave for different grid refinement levels, where the origin, X_c=0.0 corresponds to the shock location and X/m =7.6

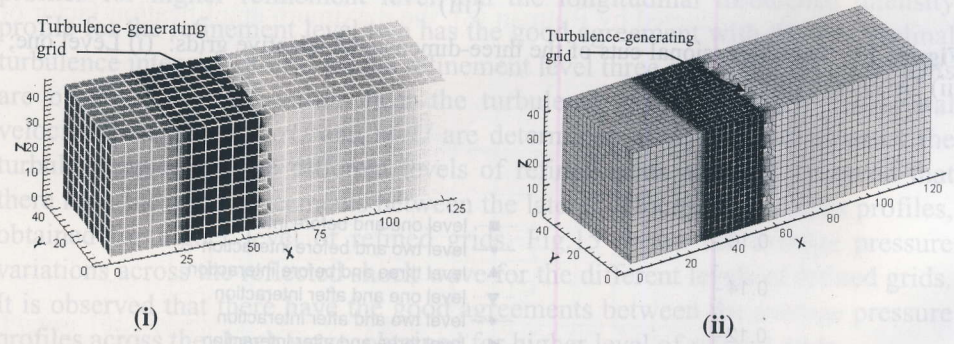

Figure 16 : Three dimensional mesh and the position of the turbulence-generating grid plate are shown where different grid sizes are (i) 2x2x2 grid/cm^3; (ii) 4x4x4 grid/cm^3

the centerline of the turbulent region, are used to determine different turbulent parameters. Each lateral plane contains several grids and the number of grid depends on the number of grid per unit volume in the turbulent region. For 4 x 4 x 4 grid, the number of grid in the lateral plane is approximately four times more than for 2 x 2 x 2 grid. The computational results for different grid sizes are compared and performed the independence test of grid size in the present simulation results. All the results, obtained before and after the shock/turbulence interaction, are used to determine the independence test of grid size. The longitudinal turbulence intensity, $<u>/U$ are determined along the centerline of the turbulent region for different grid sizes of 2 x 2 x 2 grid and 4 x 4 x 4 grid and the comparison between the characteristic profiles of the longitudinal turbulence

intensity for different grid sizes are shown in Fig.17. It is observed in Fig.17 that the characteristic profiles for different grid sizes are simulated each other and the result indicates the independency on grid size in the present computations. Similarly the lateral velocity fluctuations, v'/U and w'/U are determined along the centerline of the turbulent region for different grid sizes of 2 x 2 x 2 grid and 4 x 4 x 4 grid and it is observed that the characteristic profiles of lateral velocity fluctuations for different grid sizes are simulated each other and the simulation results are independent on the grid size. The normalized average pressure variations are determined across the reflected shock wave for different grid sizes of 2 x 2 x 2 grid and 4 x 4 x 4 grid and the comparison between the average pressure profiles for different grid sizes are shown in Fig.18. It is observed in Fig.18 that the average pressure profiles across the shock wave for different grid sizes are simulated each other and this result also indicates the independency on grid size in the present computations.

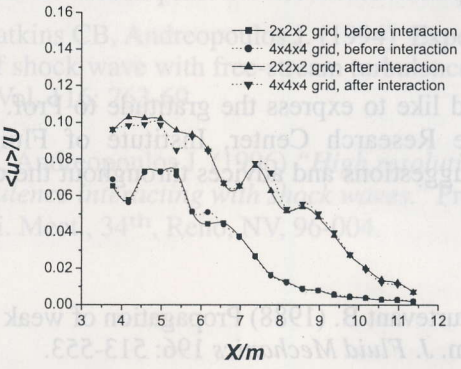

Figure 17: Longitudinal turbulence intensity *(<u>/U)* before and after the shock/turbulence interaction along the centerline of the turbulent region for different grid sizes

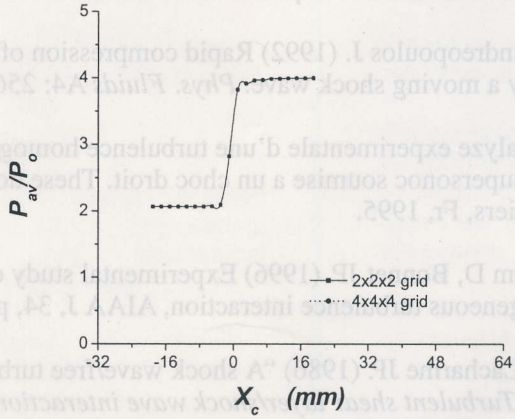

Figure 18 : Average pressure (P_{av} /P_o) variation across the reflected shock wave for different grid sizes, where, X_c= 0.0 corresponds to the shock location and *X/m* =7.6

5 CONCLUSIONS

The present computational results indicate that turbulence intensities of velocity are amplified after interaction of the shock wave with the turbulent flow. The magnitude of this amplification varies with the change of shock Mach number and the flow velocity following the shock wave. It is observed that the amplification of turbulent intensities are higher value in interaction of normal shock with the subsonic flow fields and decrease this value in interaction with the supersonic flow fields. Experimentally to find out the amplification of turbulent intensities and other parameters are the difficult tasks. In that case, computational results can be used as diagnostics tools. The present computations indicate that the amplification of turbulent kinetic energy levels are higher value in interaction of normal shock with the subsonic flow fields and decrease this value in interaction with the supersonic flow fields. After interaction, the dissipation rate of TKE decreases in all the cases of shock/turbulence interaction. Grid convergence study has been conducted in this computational work and it is observed that all computational results are independent on the grid size.

Acknowledgement

The authors would like to express the gratitude to Prof. T. Saito and Dr. M. Sun of Shock Wave Research Center, Institute of Fluid Science, Tohoku University for their suggestions and advices throughout the course of the present project.

REFERENCES

[1] Hesselink L, Sturtevant B. (1988) Propagation of weak shocks through a random medium. *J. Fluid Mechanics* 196: 513-553.

[2] Keller J, Merzkirch W. (1990) Interaction of a normal shock wave with a compressible turbulent flow. *Experiments in Fluids* 8: 241-248.

[3] Honkan A, Andreopoulos J. (1992) Rapid compression of grid-generated turbulence by a moving shock wave. *Phys. Fluids* A4: 2562-72.

[4] D. Alem. Analyze experimentale d'une turbulence homogene en ecoulement supersonoc soumise a un choc droit. These doc. Univ. de Poitiers, Poitiers, Fr, 1995.

[5] Barre S, Allem D, Bonnet JP. (1996) Experimental study of a normal shock/homogeneous turbulence interaction, AIAA J, 34, pp. 968-74

[6] Debreve JF, Lacharme JP. (1986) "A shock wave/free turbulence interaction." *Turbulent shear layer/shock wave interaction*, edited by J. Delery, Springer-Verlag, Berlin.

[7] Jacquin L, Blin E, Geffroy P. (1991) "Experiments of free turbulence/shock wave interaction. Proc. Turbulent shear flows, 8, tech Univ, Munich, Ger. pp 1-2-1-1-2-6.

[8] Rotman D. (1991) Shock wave effects on a turbulent flows. *Phys. Fluids* A, Vol. 3, No. 7: 1792-806.

[9] Lee S, Lele SK, Moin P. 1991a "Direct numerical simulation and analysis of shock turbulence interaction." *AIAA* paper 91-0523.

[10] Sun M, Takayama K. (1999) Conservative smoothing on an adaptive quadrilateral grid. *Journal of Computational Physics Vol.* 150: 143-180.

[11] Lee S, Lele SK, Moin P. (1993) Direct numerical simulation of isotropic turbulence interacting with a weak shock wave. *Journal of Fluid Mechanics* Vol. 251: 533-62.

[12] Honkan A, Watkins CB, Andreopoulos J. (1994) Experimental study of interactions of shock wave with free-stream turbulence. *Journal of Fluids Engineering*, Vol. 116: 763-69.

[13] Briassulis GK, Andreopoulos J. (1996) *"High resolution measurements of isotropic turbulence interacting with shock waves."* Presented at AIAA, Aerospace Sci. Meet., 34th, Reno, NV, 96-004.

(Contd. from 2nd cover page)

8. SI units must be used in the manuscript. However, other units may be used in parenthesis.

9. Tables should be referred to in consecutive Arabic numerical. Each table must have a table caption.

10. Line drawings must be in a form suitable for reproduction e.g., laser printout, drawn in Indian ink on white paper or on tracing paper. Photographs should have a glossy finish. Each figure must have a number and a figure caption. Elecrtonic mode is preferred.

11. References should be set out in alphabetical order of the author's last name in a list at the end of the article. They should be given in standard form as in the following examples :

(a) Journal
Bloomer G. and Wright A., "Scheduling of Vehicles from Factory to Depot." Operations Research, Vol. 12, January, pp. 590-598, 1984.

(b) Book
Best, John., and Kahn, James V., Research in Education, Prentice-Hall, New Jersey, 1986.

(c) Monograph
Syedali, M.M. "Computer Controlled Car", Thesis, M.Sc. Engineering, Department of Mechanical Engineering, BUET, 1990

(d) Conference Paper
Hasan, M. and Ullah, M.S. "Tourism development in the Chittagong Hill Tracts of Bangladesh after the peace agreement of 1997", a paper submitted to the Regional Conference on physical mobility and development in the mountains", Tribhuvan University, 15-17, March, 2000 Kathmandu, Nepal, pp.12

(e) Unpublished paper
Ahmadi, R and Tangs : Production Allocation with Dual Provisioning, Working Paper, Anderson Graduate School of Management, UCLA (1991)

12. The University does not accept responsibility for loss or damage of manuscript while in mail.

13. The responsibility for opinions in the contributions rests entirely on their authors.

14. The author (s) must submit declaration that the paper was not published elsewhere.

15. In case of joint papers, communication will be made with the first author.

16. The University will reserve the copyright of the paper once it is accepted for publication in the Journal. The authors must obtain written parmission from REASP, IUT for publication elsewhere.

Procedure for acceptance of papers and publications :

1. Papers submitted for publication will be referred to the listed reviewers for assessment. However, the editorial board will make initial screening of the papers.

2. After the assessment, the authors may be requested to modify/clarify certain points.

3. Accepted/modifed/corrected papers will be published in the next issue of the Journal.